ELSEVIER

Brain Research 877 (2000) 209–217

BRAIN RESEARCH

www.elsevier.com/locate/bres

Research report

Assessing accurate sizes of synaptic vesicles in nerve terminals

Seongjai Kim[a,*], Harold L. Atwood[b], Robin L. Cooper[c]

[a]*Department of Mathematics, University of Kentucky, Lexington, KY 40506-0027, USA*
[b]*Department of Physiology, University of Toronto, Toronto, Ontario, Canada 5MS-1A8*
[c]*Thomas Hunt Morgan School of Biological Sciences, Nerve–Muscle Research Group, and Center for Ecology, Evolution and Behavior, University of Kentucky, Lexington, KY 40506-0225, USA*

Accepted 27 June 2000

Abstract

Chemical synaptic transmission occurs when vesicles within a presynaptic neuron fuse to the membrane and release their neurotransmitter content into the synaptic cleft, eliciting a response in the postsynaptic cell. If concentration of neurotransmitter is the same in all synaptic vesicles, the volume of the vesicle determines how much transmitter is released. Thus, variation in vesicular volume may contribute to observed variance of synaptic quantal unit size. The present study provides an approach to more fully and accurately characterize the dimensions of synaptic vesicles within a population containing varied sizes of vesicles. The methodology can be applied in a wide range of stereological problems. The approach characterizes the distribution of vesicle sizes within a population and provides a means to assess effects of experimental manipulations on vesicle dimensions. The mathematical treatments to obtain the true distribution of vesicle sizes involve extraction of the observed distribution from an enlarged population containing smaller vesicle diameters produced by sectioning of the specimens. A FORTRAN program is provided.

Theme: Excitable membranes and synaptic transmission

Topic: Presynaptic mechanisms

Keywords: Synapse; Nerve terminal; Stereology; Numerical integration; Algebraic system

1. Introduction

Chemical synaptic transmission occurs when vesicles within a presynaptic neuron fuse to the membrane and release their contents into the synaptic cleft, activating receptors on a postsynaptic cell. The amount of transmitter released depends on the number of vesicles that fuse and the amount of transmitter packaged within the vesicles. The size of synaptic vesicles is one of the limiting factors for packaging transmitter and thus there has been an interest in descriptive analysis of vesicular size in a variety of preparations [10]. Genetic alterations of identified proteins in *Drosophila* have given rise to populations with large vesicles (within the terminal) as a result of vesicles not being able to recycle. The synaptic physiology of such mutations is correspondingly altered [9]. On the other hand, small vesicles are more apparent in those nerve terminals that have experienced enhanced activity as compared to those with a quiescent synapse, within the same type of neuron in the same animal [8,11]. This suggests that recycling rates may have an effect on the dimensions of synaptic vesicles. In all nerve terminals examined in which distributions of vesicle size have been reported, there is a clear indication that vesicle populations are non-uniform with respect to vesicle size.

Neuroendocrine cells that release hormones and peptides typically contain vesicles of larger diameters than those at classical synapses [5]. Although dense-cored vesicles which contain peptides are found within nerve terminals of non-neuroendocrine cells, they occur with lower frequency than the clear-cored vesicles which contain neurotransmitter [7]. The distinction of ‘dense’- and ‘clear’-cored vesicles arises due to the electron density of stained

*Corresponding author. Tel.: +1-606-257-8681; fax: +1-606-257-4078.

E-mail address: skim@ms.uky.edu (S. Kim).

0006-8993/00/$ – see front matter
PII: S0006-8993(00)02641-X

material observed with electron microscopy. Dense-cored vesicles are typically larger than clear-cored vesicles, but stereological problems arise in making such distinctions.

Many investigators report *mean diameters* of vesicles measured from electron micrographs for obtaining an index of vesicle dimensions and for making comparisons among experimental samples. The mistake in reporting a 'mean diameter' as such is that it is very misleading and in error since it does not reflect the true diameters of vesicles. This mean value is obviously not the mean diameter of the vesicles present, but a mean of the distribution of sectioned vesicles projected from a 3-D to a 2-D plane, i.e., a photomicrograph. Obtaining true diameters of vesicles is difficult since they are small and must be visualized on micrographs obtained by electron microscopy.

To obtain electron micrographs, the experimental tissue should be sectioned within a range of 50–100 nm in thickness. Since sectioning of vesicles is random, they are sectioned at various planes whileother vesicles may reside between the sectioning planes, depending on section thickness and vesicle dimensions. Stereological complexity arises when spherical vesicles are sectioned with less than half or just the caps (i.e., ends) remaining within a section. These less than half sections of the vesicles will give rise to various sized projected circular images. When half or more of the spherical vesicle resides within the section, the true diameter of the sphere will be represented in the projected image. If the projected 2-D circles are measured as representing vesicle diameters, then the data are degraded by the less than true sized projections and will misrepresent mean diameter to be less than the true dimensions. If the vesicles were all of a given size, then the true diameters would be the largest values obtained. This would be represented in a plotted distribution of random sections as the predominant values of the largest diameters. But as already mentioned, vesicles appear to be truly of mixed sizes within nerve terminals. This results in misleading information by the reporting of mean values of degraded distributions obtained by projections of the different sized vesicles. One further methodological issue is the fact that when the very ends of vesicles are sectioned, the small projected circles may not be resolved in electron micrographs from background staining of the cell's cytoplasm and other organelles, and thus are not resolved as parts of vesicles. These stereological issues for spheres have been addressed in the past, but on a mathematical basis which did not address the practical aspects associated with biological relevance to obtained data [4].

The present study applies mathematical principles to determine the percentage of different sized vesicles within a mixed population, taking into account degradation of the data for stereological projections of parts of vesicles. The usefulness of this approach is amplified by the inclusion of an algorithm that can be run on personal computers and work stations.

2. Mathematical and numerical formulations

For the present study, a mathematical formula has been developed to address the relationship between the true distribution and the observed distribution of the vesicle sizes. This is a revision of the formula Goldsmith [4] developed to handle arbitrarily scaled distributions. It is a Volterra integral equation of the second kind. For an accurate numerical computation of true vesicle distribution, the (fourth-order accurate) Simpson's Rule was applied to the revised formula.

The following formula's variables include:

t: thickness of the viewing slice
X: maximum diameter of vesicle size
x: variable for vesicle diameters
$f(x)$: the true distribution of vesicle sizes
$g(x)$: the observed distribution of vesicle sizes

It is assumed that particle sizes are continuously distributed. The normalized distribution of f is defined by

$$\tilde{f}(x) = \frac{1}{\|f\|_1} f(x), \quad \|f\|_1 = \int_0^X f(x)\,\mathrm{d}x,$$

where $\|f\|_1$ is the $L^1(0, X)$-norm of f. Thus is obtained the following formula:

$$g(x) = \frac{1}{\kappa}\left(tf(x) + x\int_x^X \frac{f(y)\,\mathrm{d}y}{(y^2 - x^2)^{1/2}} \right), \tag{1}$$

where

$$\kappa = t + m, \quad m = \int_0^X x\tilde{f}(x)\,\mathrm{d}x.$$

Note that when $\|f\|_1 = 1$, the formula (1) becomes the one presented in [4]. A few interesting solution procedures are presented in [4] for the relative distribution of $\tilde{f}$.

The second objective is to introduce a numerical scheme for (1) which is accurate and easy to understand and utilize. Let $h = X/n$ for a positive integer n and

$$x_i = ih, \quad i = 0, 1, \ldots, n.$$

Define the average frequencies on each of the subintervals $[x_{i-1}, x_i]$, $i = 1, \ldots, n$:

$$f_i = \frac{1}{h}\int_{x_{i-1}}^{x_i} f(x)\,\mathrm{d}x, \qquad g_i = \frac{1}{h}\int_{x_{i-1}}^{x_i} g(x)\,\mathrm{d}x.$$

The quantity κ is constant; it is momentarily treated as a known value. Multiplying (1) by κ, and integrating the resulting equation over the interval $[x_{i-1}, x_i]$ results in

$$\begin{aligned}\kappa h g_i &= h t f_i + \int_{x_{i-1}}^{x_i} x\,\mathrm{d}x \int_{x}^{X} \frac{f(y)\,\mathrm{d}y}{(y^2 - z^2)^{1/2}} \\ &= h t f_i + \int_{x_{i-1}}^{x_i} x\,\mathrm{d}x \int_{x}^{x_i} \frac{f(y)\,\mathrm{d}y}{(y^2 - x^2)^{1/2}} \\ &\quad + \int_{x_{i-1}}^{x_i} x\,\mathrm{d}x \int_{x_i}^{X_i} \frac{f(y)\,\mathrm{d}y}{(y^2 - x^2)^{1/2}} \\ &= h t f_i + \int_{x_{i-1}}^{x_i} f(y)\,\mathrm{d}y \int_{x_{i-1}}^{y} \frac{x\,\mathrm{d}x}{(y^2 - x^2)^{1/2}} \\ &\quad + \int_{x_i}^{X} f(y)\,\mathrm{d}y \int_{x_{i-1}}^{x_i} \frac{x\,\mathrm{d}x}{(y^2 - x^2)^{1/2}} \\ &= h t f_i + \int_{x_{i-1}}^{x_i} (y^2 - x_{i-1}^2)^{1/2} f(y)\,\mathrm{d}y \\ &\quad + \int_{x_i}^{X} [(y^2 - x_{i-1}^2)^{1/2} - (y^2 - x_i^2)^{1/2}] f(y)\,\mathrm{d}y \\ &\approx h t f_i + b_{ii} f_i + \sum_{j=i+1}^{n} (b_{ij} - b_{i+1,j}) f_j \end{aligned} \tag{2}$$

where

$$b_{ij} = \int_{x_{j-1}}^{x_j} (y^2 - x_{i-1}^2)^{1/2}\,\mathrm{d}y, \quad j = i+1, \ldots, n.$$

For the computation of b_{ij}, the Simpson's Rule is employed as follows:

$$\begin{aligned} b_{ij} \approx \frac{h}{6} \{ &(x_{j-1}^2 - x_{i-1}^2)^{1/2} + 4((x_{j-1} + h/2)^2 - x_{i-1}^2)^{1/2} \\ &+ (x_j^2 - x_{i-1}^2)^{1/2} \}. \end{aligned} \tag{3}$$

Then, the algebraic system for (2) reads

$$A\hat{\mathbf{f}} = \mathbf{g}, \tag{4}$$

where

$$A = \begin{bmatrix} a_{11} & a_{12} & a_{13} & \cdots & a_{1n} \\ & a_{22} & a_{23} & \cdots & a_{2n} \\ & & \ddots & \cdots & \vdots \\ & 0 & & & a_{nn} \end{bmatrix},$$

$$\hat{\mathbf{f}} = \frac{1}{\kappa} \begin{bmatrix} f_1 \\ f_2 \\ \vdots \\ f_n \end{bmatrix}, \qquad \mathbf{g} = \begin{bmatrix} g_1 \\ g_2 \\ \vdots \\ g_n \end{bmatrix}.$$

Here the nonzero elements of A are defined as

$$a_{ii} = t + b_{ii}/h; \qquad a_{ij} = (b_{ij} - b_{i+1,j})/h, \quad j = i+1, \ldots, n.$$

The upper triangular system (4) can be easily solved for $\hat{\mathbf{f}}$ by the back substitution. A FORTRAN code is provided in Appendix A.

It is necessary to find m to determine f out of $\hat{\mathbf{f}}$. Let $\hat{f}(x)$ denote the functional representation of $\hat{\mathbf{f}}$. Then, it is easy to see that the mean of $\tilde{f}$, m, is the same as that of $\hat{f}$. In fact,

$$\hat{f}(x) = \frac{f(x)}{t+m} = \frac{\|f\|_1}{t+m}\,\tilde{f}(x), \qquad \int_0^X \tilde{f}(x)\,\mathrm{d}x = 1,$$

and

$$\int_0^X \hat{f}(x)\,\mathrm{d}x = \int_0^X \frac{f(x)}{t+m}\,\mathrm{d}x = \frac{\|f\|_1}{t+m},$$

$$\int_0^X x\hat{f}(x)\,\mathrm{d}x = \int_0^X x\,\frac{\|f\|_1}{t+m}\,\tilde{f}(x)\,\mathrm{d}x = \frac{\|f\|_1}{t+m}\,m.$$

Therefore, m is found as the mean of $\hat{f}(x)$:

$$m = \int_0^X x\hat{f}(x)\,\mathrm{d}x \Big/ \int_0^X \hat{f}(x)\,\mathrm{d}x. \tag{5}$$

Note that $\hat{f}(x) = \hat{f}_i$ for $x_{i-1} \le x < x_i$. So the exact formulas can be utilized for the computation of $\int_0^X \hat{f}(x)\,\mathrm{d}x$ and $\int_0^X x\hat{f}(x)\,\mathrm{d}x$ as follows:

$$\begin{aligned} \int_0^X \hat{f}(x)\,\mathrm{d}x &= h \sum_{i=1}^{n} \hat{f}_i \\ \int_0^X x\hat{f}(x)\,\mathrm{d}x &= \frac{h}{2} \sum_{i=1}^{n} (x_{i-1} + x_i)\hat{f}_i. \end{aligned} \tag{6}$$

By multiplying $\hat{\mathbf{f}}$ by $(t+m)$, which is now known, one can recover the true distribution $\mathbf{f}$.

It also should be noted that the data may not guarantee a nonnegative solution $\hat{\mathbf{f}}$. The solution can be adjusted as nonnegative in each step of the back substitution (4), rather than adapting after finishing all steps of the back substitution. See the code in Appendix A.

3. Data acquisition

All experiments were performed on the abdominal slow flexor muscle in the crayfish, *Procambarus clarkii* (Atchafalaya Biological Supply Co., Raceland, LA). Preparations were dissected in a modified Van Harreveld's crayfish solution, followed by rapid processing for electron microscopy [6]. Sections were collected on Formvar-coated slotted grids. A log of each serial section was kept and the thickness was determined by interference colors of the

sections while they were floating on the surface of water after sectioning. Sections were for the most part consistently cut at 75 nm. The sections were viewed and photographed on an electron microscope at a magnification of seven times followed by printing at a magnification of 20 600 times. Calibrations were made by the use of calibrated electron microscopic grids for each magnification setting. Measurements of synaptic vesicle diameters were made by a single individual with the use of an eye micrometer.

Fox [3] reported that the greatest amount of error in measurement of synaptic vesicle diameters occurred between various individuals. Therefore sampling error can be reduced by the use of a single individual for a set of data and using enlarged micrographs to obtain the measures. The outermost thickness of the vesicle membrane was taken as the diameter. To determine if the vesicles were of a uniform diameter, perpendicular measures were made across the projected vesicle image. The projected circles taken for this study were for the most part uniform in their horizontal and vertical dimensions.

4. Results

The stereological issue involving randomly sectioned spheres is exemplified by the projections of the ends of vesicles which are caught within a section of interest. This is diagrammatically illustrated in Fig. 1, in which randomly placed spheres of two different diameters are sectioned at various locations. The fragments that are over half of the vesicle within the section project as true diameters, whereas the smaller fragments, less than half of vesicle size, produce projected circles of less than the true vesicle diameters. This can produce projected views that overlap in the dimensions between the two different sized original vesicle sizes. Some of the fragments from vesicles 50 nm in diameter may not be distinguished from those obtained from the original 37 nm diameter vesicles.

The thickness of a section will alter the number of vesicles observed depending on their density in the medium. As can be seen in Fig. 2, when the density is high within a section, the overlapping projected images in the line of the electron beam will produce obscure views of the vesicle dimensions. An optimal section thickness may have to be devised for the sample in question. Here at the crayfish neuromuscular junction, 75 nm is sufficient to avoid overlap of projected vesicle images within a section.

If one plotted the distribution of the 2-D projections of spheres as shown in Fig. 1 for a single-sized vesicle population in a large number of sections, then a (synthetic) graphical representation would be as indicated in Fig. 3; see Eqs. (1) or (2) for a mathematical expression. This theoretical distribution of random sectioning of a sphere for one given diameter would provide the true diameter of the sphere as the largest values for diameter, i.e., on the right end of the distribution. The fragmented pieces give rise to the left end of the distribution, which drops in the number of occurrences for the smaller fragments. This indicates that the smallest fragments would occur less in frequency than the larger fragments, in particular when half or more of a sphere is contained within a section.

Combining two populations of spheres used for the illustrative problem in Fig. 1 into the same space would result in an additive distribution, with the overall probability larger for the peak of the smaller spheres because of the addition of the fragmented projections for the larger spheres (see Fig. 4).

Within a section of the crayfish motor nerve terminal that was imaged with an electron microscope, one can readily resolve the image of many vesicles with various projected diameters, as shown in Fig. 5. A substantial number of these projections are likely to be fragments from sections of the vesicles. The majority of the vesicles seen are the clear core vesicles (CCV) and relatively few dense core vesicles (DCV). Other structures, such as mitochondria and the synapse, are shown.

From several sections of the same muscle and its associated terminals, the projected diameters of what appeared to be CCV were plotted as the thin curve in Fig. 6. The distribution is truncated on the left-hand side because of the inability to resolve fragments of vesicle from background tissue and staining in the micrographs. This is one of the major differences between the theoretical distributions (as shown in Figs. 3 and 4) and the distributions obtained from biological tissue, not previously considered in mathematical assessments of stereological problems. In order to account for the additive effect of underlying distributions, the present study uses the Simpson's Rule as the numerical integration on each of 48 subintervals along the probability function curve for the observed distribution. This results in an algebraic system of an upper triangular matrix, as discussed in Section 2. Solving the algebraic system by the back substitution is exactly the same as removing the additive effect of underlying distributions. Since the biological data set is truncated at the lower diameters and data are not present, subtraction of the theoretical distributions within this range would result in negative values. Therefore, the distribution subsequent to subtraction should be appropriately adjusted to have nonnegative values during the back substitution. This modification is necessary and practical for biological tissue assessment. The resultant distribution is plotted as the thick curve in Fig. 6.

The probability distribution can now be used to assess the ranges of vesicle size and their relative contribution to the entire population; see Fig. 7. The binning of the distribution is based on the valleys within the adjusted (true) distribution. Such a binning procedure can be used for comparisons among treatments, which may affect

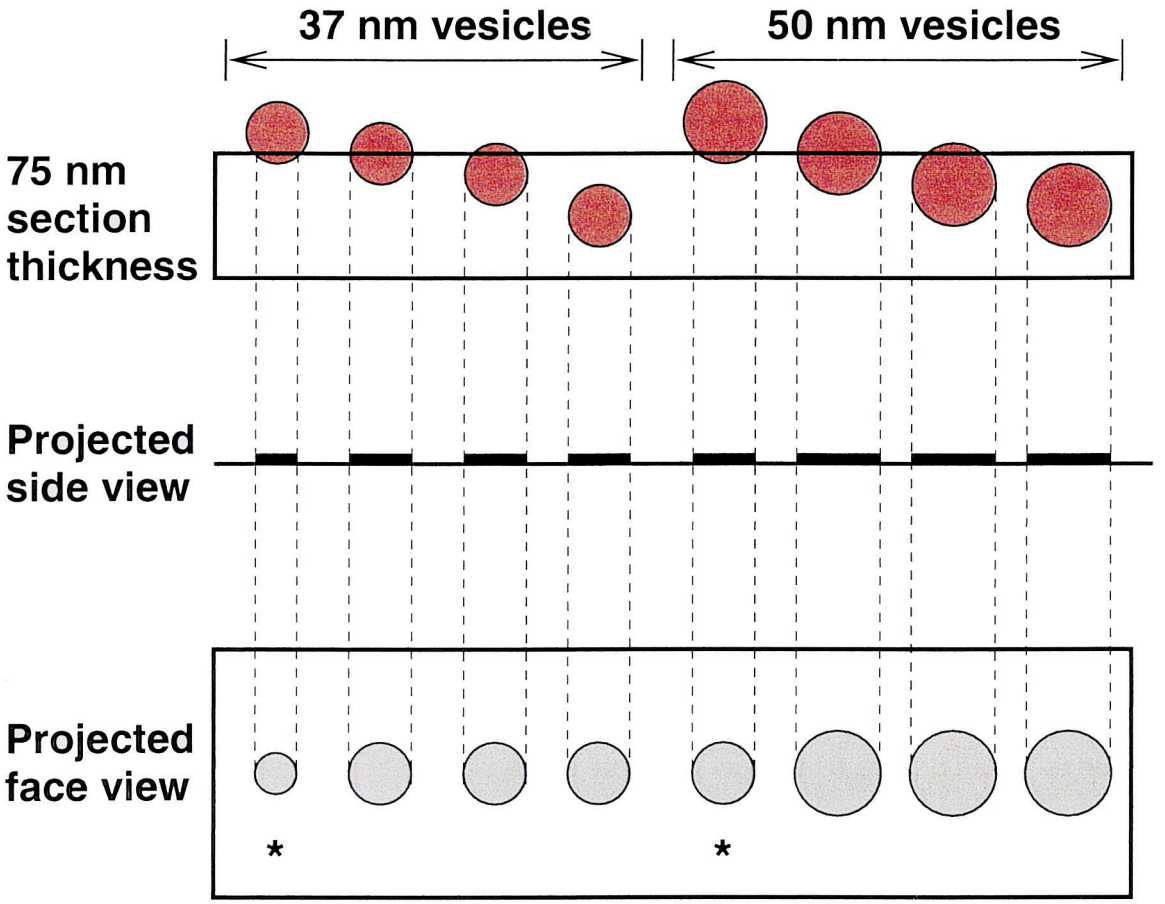

Fig. 1. Spheres of two different sizes (37 nm and 50 nm) are placed randomly in space. A section of 75 nm in width is shown through this space. The projected images of the sectioned spheres are shown in 2-D surface. A range in projected circle diameters from the section are shown in side and face view.

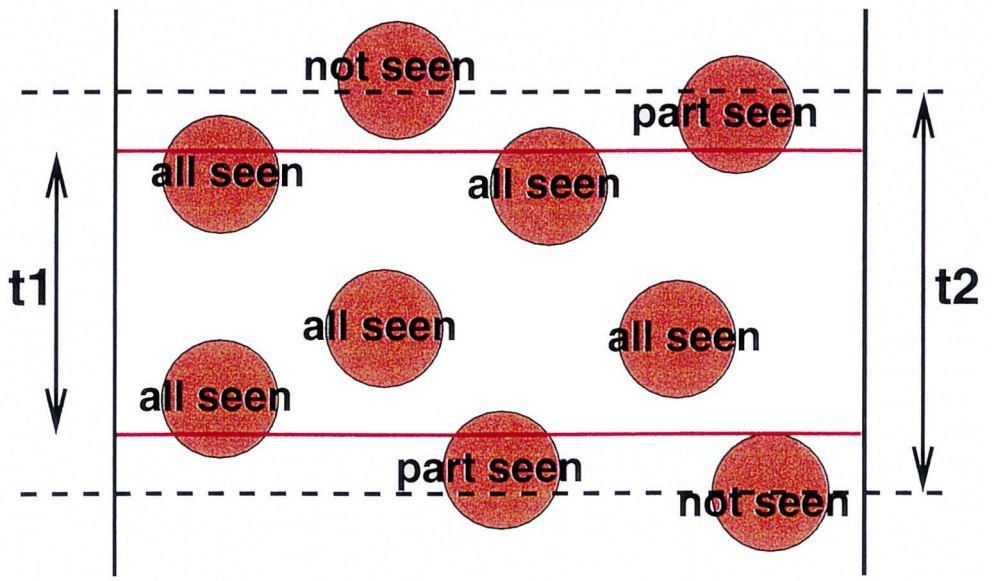

Fig. 2. It is important to determine optimal section thickness, in order to prevent overlap of projected images. This can readily be determined by section thickness close to the size of the thickness of the objects of interest. For synaptic vesicles at the crayfish neuromuscular junction, 75 nm is sufficient. The lengths $t1$ and $t2$ denote the thickness of the sections.

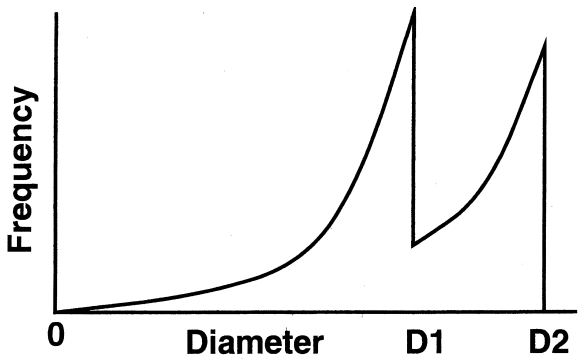

Fig. 4. When two different vesicle populations exist within the same space, then the combined probability functions would appear as shown. The distribution of the smaller sized vesicles is offset to include a larger number of occurrences, due to the additional data gathered from the larger diameter vesicle population.

synaptic vesicle dimensions or comparative studies among different types of nerve terminals.

The groupings in vesicle sizes are easily tabulated and compared for absolute number of occurrences or percentages of the total population, as in Table 1. Since the fragmented projections of the larger vesicles are removed in the adjusted data, the adjusted number of occurrences become smaller than those in the raw data; the total number of measurements in the raw data is 932, while the adjusted data contain 695 measurements in total. The left-hand portion of the fourth column contains the percent differences between raw and adjusted data. (A minus indicates a decrease in the adjusted data as compared with the raw data). The distributions are reduced more substantially for smaller vesicle sizes, which is expected from the algebraic system (4). The right-hand portion of the fourth column shows the differences between the percent in distributions of the adjusted and raw data. For vesicles larger than or equal to 38.2 nm, the percent indistribution increase in the adjusted data set.

Prior studies in reporting vesicle diameters have used

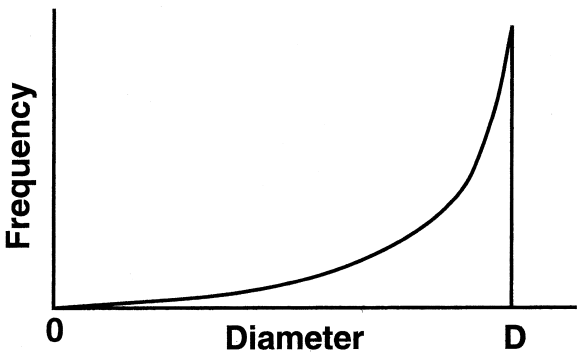

Fig. 3. The theoretical distribution of random sectioning of a sphere for one set diameter would result in a probability histogram with the true diameter of the vesicles being the values furthest to the right (i.e. *D*).

the mean of the distributions obtained from vesicle fragments as well as whole vesicles, without concern for the stereological issues. To compare differences in the entire distribution before (Fig. 7(a)) and after (Fig. 7(b)) adjustment of additive distributions, we calculated the mean for the two distributions: 40.7 and 41.7, respectively. The adjustment of the distribution provides a larger mean diameter than obtaining the value from the raw data set.

5. Discussion

This study presents an approach for characterizing the dimensions of synaptic vesicles in a population of varied sizes that would typically be contained in presynaptic nerve terminals. The foundation of the methodical procedures is fundamental to a wide range of applications of stereological based problems. The dimensions of vesicles are key to the amount of neurotransmitter that can be packaged and available for transmission. Thus, the size of vesicles is suggested as the mechanism behind the observed variability in quantal responses of synaptic currents [9,10]. The approach used in this study allows investigators to readily index the potential distribution in vesicle size within a population. By obtaining the relative percentages of vesicle sizes, any experimental manipulation can be assessed as to the effects on the dimensions of vesicles, or can be compared to physiological measures for structure–function studies. In addition, the provided FORTRAN program allows the computational analysis to be performed on personal computers as well as work stations.

Studies which report a single value, a mean diameter, of the projected vesicle profiles are not informative and are misleading, considering that the profiles contain fragments of vesicles and that the populations are likely to be made up of vesicles of truly varied diameters. Approaches that represent the entire distributions of vesicle profiles need to be tackled, so that more complete assessments can be obtained. By dividing the distribution of the vesicle diameter profiles, as in Fig. 7, a finer resolution for indexing the overall distribution is possible. The mean, standard deviation, standard error and the percent of occurrences of the total can readily be obtained for each subset (i.e., bin) for comparisons within the sample as well as among preparations, to better assess experimental conditions or structure–function considerations.

The sizes of vesicles in nerve terminals have been shown to be altered by fixation procedures. Thus comparative studies should be performed with the same conditions [3]. Although Fox reported skewness and kurtosis for the entire distribution of vesicle profiles, better information could be gained if the fractions within the population were reported. This would help determine if fixation artifacts had a more noticeable effect for a particular subset of the population. When examining osmolarity or fixation con-

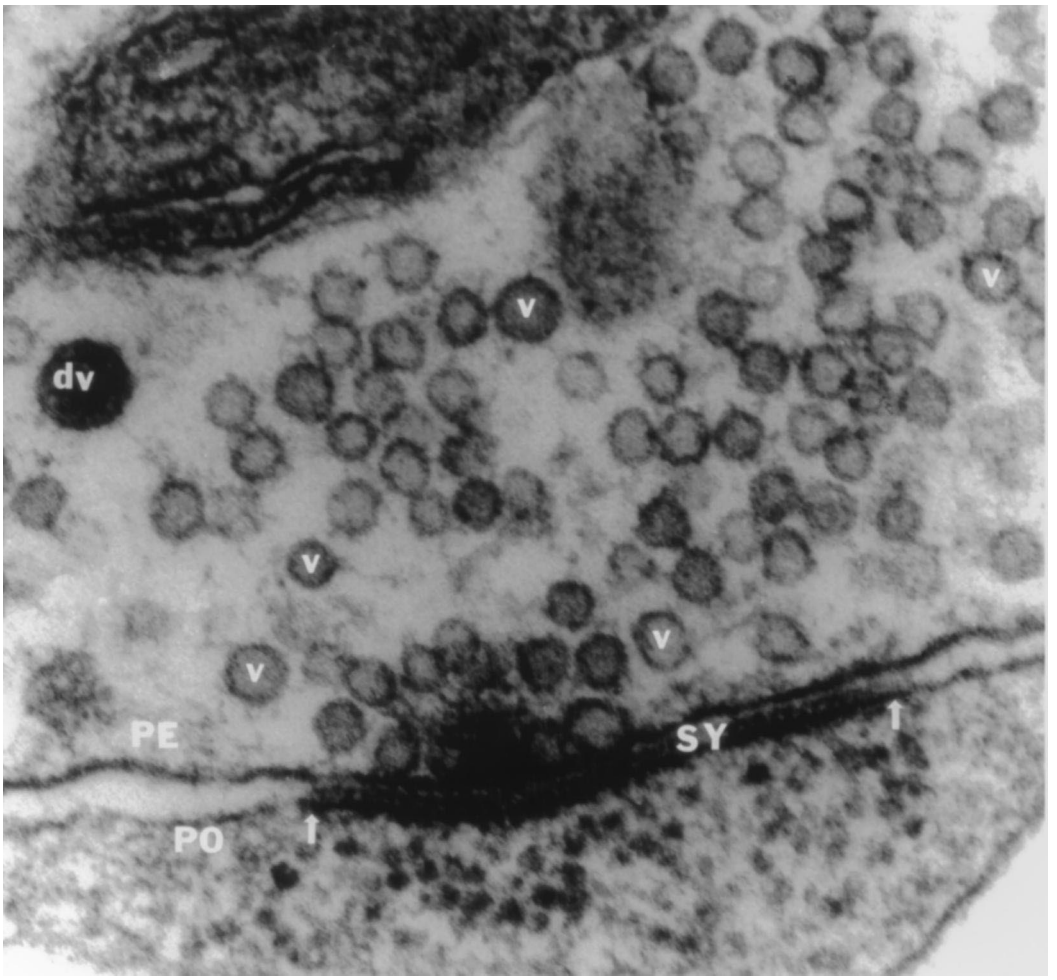

Fig. 5. An electron micrograph of a motor nerve terminal. The apposition of the pre- and post-synaptic thickening defines the synapse. On the synapse a dark body attached to the synapse that rises up into the cytoplasm is the dense body in which synaptic vesicles will line up around, to fuse with the presynaptic membrane. The spherical objects within the presynaptic terminal are clear core vesicles (CCV). The dark, enlarged vesicle in the upper left is a dense core vesicle (DCV). A mitochondrion is also shown in this image.

Table 1
The raw and adjusted (true) distributions of the occurrences in projected diameters can be compared by subdividing the population into sets which contain normal deflections in the distribution, or by unitary divisions[a]

Diameter		Raw data		Adjusted		Differences (%)	
23.0	32.7	98	10.5%	41	5.9%	−58.2	−4.6
32.7	38.2	247	26.4%	175	25.1%	−29.1	−1.3
38.2	45.2	346	37.1%	275	39.5%	−20.5	2.4
45.2	47.9	104	11.2%	87	12.5%	−16.3	1.3
47.9	57.7	127	13.6%	108	15.6%	−15.0	2.0
57.7	67.0	10	1.1%	9	1.3%	−10.0	0.2

[a] The adjusted distribution was divided into groupings based on the valleys within natural population. The same unitary division was applied to the raw distribution. The occurrence numbers and their percentages are compared. In the fourth column, the percent difference in the left-hand portion is calculated by the formula [100 · (Adjusted − Raw)/Raw], while the right-hand portion is differences between percent distributions of adjusted and raw data

ditions, it is conceivable that vesicles with a larger volume to surface area would exhibit a greater alteration. Fluctuations measured in synaptic quantal currents from either spontaneous or evoked events remain in debate as to the underlying mechanisms. See [2] for a review on the topic, which includes cases presented for the presynaptic and postsynaptic factors that regulate the sizes of synaptic quantal currents.The presynaptic reasons involve either transmitter packaging within a given vesicle or variability of vesicle size, which also limits the packaging of neurotransmitter.

A small change in the vesicle diameter can result in significant differences in volume of the vesicle. Since the size may limit the amount of transmitter that can be packaged within a vesicle, the size may be a factor which and regulated the extent of synaptic transmission that can take place. In a preparation like the crayfish neuromuscular

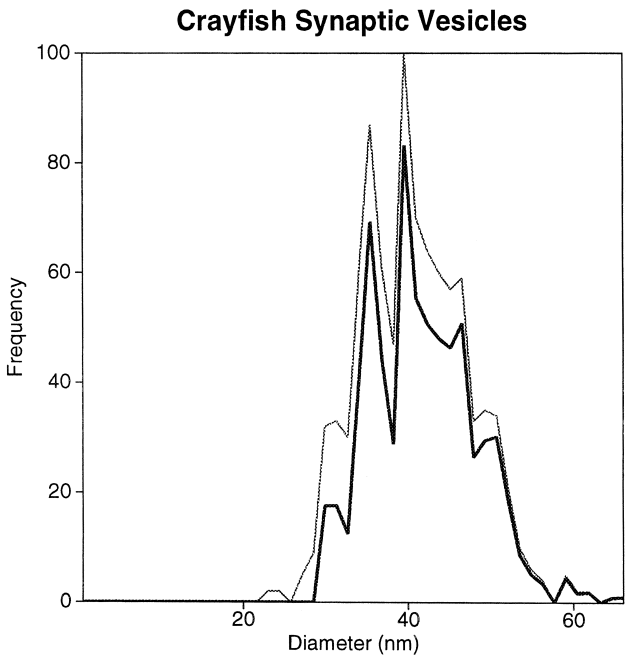

Fig. 6. The thin curve indicates the observed distribution, while the thick curve is the true distribution obtained by solving the algebraic system (4). The section thickness is 75 nm.

junction, a direct structure–function analysis is feasible, because discrete regions of neuromuscular junctions can be recorded for synaptic currents. Those same regions can be marked for subsequent serial reconstruction at the electron microscopic level [1]. Although the vesicles that give rise to the physiological responses cannot be directly correlated, the population in which they arose can be measured.

The mathematical treatment of continuous removal of the observed distribution from the enlarged population of smaller vesicle diameters is beneficial in that it reveals the contribution of each size range to the overall distribution, without obscuring the measures through contamination of the larger profiles. Goldsmith [4] approached this stereological problem of spheres in the theoretical realm, and devised a closed form solution for the left hand side of a distribution. Assessment of the truncated data on the left side in the distribution for small diameter profiles is not possible, because the data sets are missing. Under certain conditions one can be confident that small circular structures that appear in electron micrographs arise from vesicles and this can assist the researcher in obtaining a more complete representation of the fragments of vesicles. However there is also the problem that the vesicle membrane may not be electron-dense enough to be differentiated from background in electron micrographs. For these reasons, the data set for the smallest of profiles cannot be measured in practice. For a more correct assessment, the region within the histograms for the absent data sets should be set aside, and the mathematical calculations should be applied to the observed data.

This report has demonstrated that taking the mean in a measured distribution of vesicles diameters does not inform one on the true diameter of the vesicles nor does it inform one if various populations of vesicles sizes are present. By presenting histograms of the measurable vesicle diameters one can better estimate if various populations exist and at what percentage within the entire distribution. This report allows one to better assess the true population of vesicle diameters in estimating a distribution without additive effects due to stereological artifacts of measure.

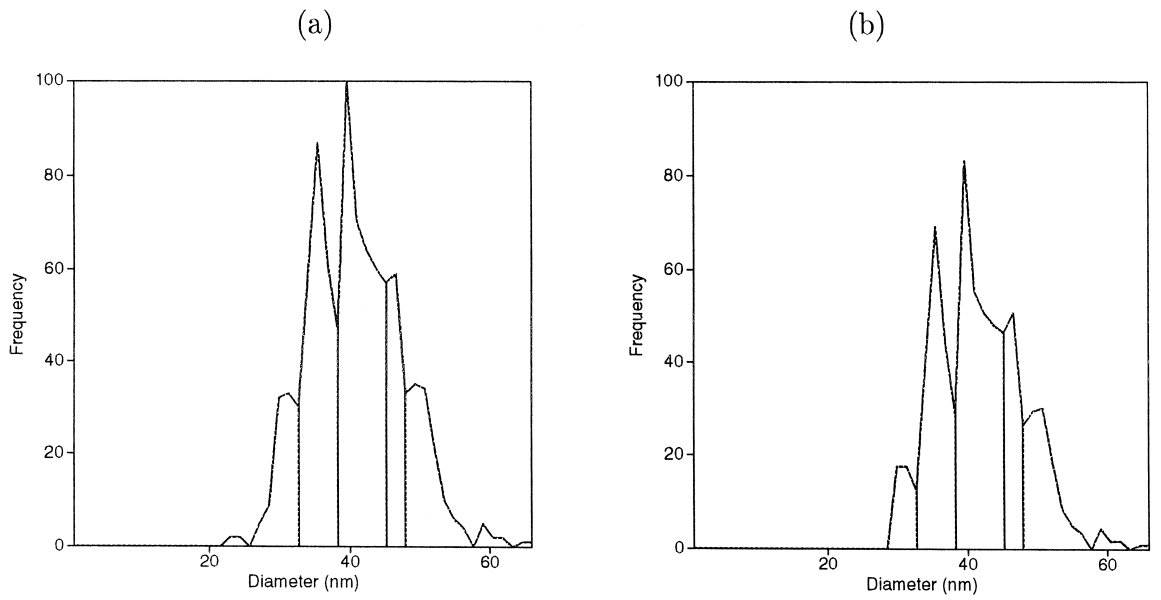

Fig. 7. Binning for comparative studies. The binning of the distribution is based on the valleys within the adjusted (true) distribution.

Acknowledgements

We thank Mr. Leo Marin for tissue processing and photomicrographs of tissue, and anonymous referees for their helpful suggestions that improved the quality of the manuscript. H.L.A. and R.L.C. have been partially supported by NSF grant IBN-9808631 (RLC) and MRC-Canada (HLA).

Appendix A. A FORTRAN program

The following is a FORTRAN program for the algebraic system (4). It was used to obtain the results presented in this article. We hope it is useful for others.

```
!=======================================================================
      subroutine particle(thick,nx,idata,level,nd,A,b,x,DATA)
!=======================================================================
!---- "DATA(.)" includes the "measured diameters" in a column
!---- "idata" is the indicator for various data sets
!---- "level" is the level of stdout; the higher, the more
      implicit real*8(a-h,o-z)
      real*8 A(nx,nx),b(nx),x(0:nx)
      real*4 DATA(nd)
      if(level.ge.1) print'("PARTICLE: idata=",i2)',idata
      if(level.ge.2) print*,"nd=",nd," nx=",nx," thick=",thick
!---- check the "DATA"
      dmin=1.d10
      dmax=0.d0
      do i=1,nd
         dmin=min(dmin,DATA(i))
         dmax=max(dmax,DATA(i))
      enddo
      dx=dmax/dble(nx)
      if(level.ge.2) print*,"dmin=",dmin," dmax=",dmax," dx=",dx
!---- the points "x" and the right-hand side "b"
      do 10 i=0,nx
 10      x(i)=dble(i)*dx
      do 20 i=1,nx
 20      b(i)=0.d0
      do i=1,nd
         n0=min(int(DATA(i)/dx)+1,nx)
         b(n0)=b(n0)+1.d0
      enddo
!---- compose the matrix "A"
      do i=1,nx
         A(i,i)=thick+bij(i,i,nx,dx,x)/dx
         do j=i+1,nx
            A(i,j)=(bij(i,j,nx,dx,x)-bij(i+1,j,nx,dx,x))/dx
         enddo
      enddo
!---- back substitution
      b(nx)=b(nx)/A(nx,nx)
      do i=nx-1,1,-1
         do j=i+1,nx
            b(i)=b(i)-A(i,j)*b(j)
         end do
        b(i)=b(i)/A(i,i)
        b(i)=max(0.d0,b(i))  !!get rid of negative values
      end do
      return
      end
!=======================================================================
      real*8 function bij(i,j,nx,dx,x)
!=======================================================================
      implicit real*8(a-h,o-z)
      real*8 x(0:nx)
      xb2=x(i-1)**2
      y0=x(j-1)
      y2=x(j)
      y1=0.5d0*(y0+y2)
      bij=(dx/6.d0)*(dsqrt(max(0.d0,y0**2-xb2))     !!Simpson's Rule
     &   +4.d0*dsqrt(y1**2-xb2)+dsqrt(y2**2-xb2))
      return
      end
```

References

[1] R. Cooper, L. Marin, H. Atwood, Synaptic differentiation of a single motor neuron: conjoint definition of transmitter release, presynaptic calcium signals, and ultrastructure, J. Neurosci. 15 (1995) 4209–4222.
[2] D. Faber, H. Korn, J. Redman, S. Thompson, J. Altman, Central synapses: Quantal mechanisms and plasticity, in: Workshop IV. Human Frontier Science Program, Strasbourg, France, 1998.
[3] G. Fox, A morphometric analysis of synaptic vesicle distributions, Brain Res. 475 (1988) 103–117.
[4] P. Goldsmith, The calculation of true particle size distributions from the sizes observed in a thin slice, Br. J. Appl. Phys. 18 (1967) 813–830.
[5] T. Hökfelt, O. Johansson, A. Ljungdahl, J. Lundberg, M. Schultzberg, Peptidergic neurons, Nature 284 (1980) 515–521.
[6] S. Jahromi, H. Atwood, Three-dimensional ultrastructure of the crayfish neuromuscular apparatus, J. Cell Biol. 63 (1974) 329–334.
[7] I. Kupfermann, Functional studies of cotransmission, Physiol. Rev. 71 (1991) 683–732.
[8] V. Petukhov, V. Popov, Quantitative analysis of ultrastructural changes in synapses of the rat hippocampal field CA3 in vitro in different functional states, Neurosci. 18 (1986) 823–835.
[9] J. van de Goor, M. Ramaswami, R. Kelly, Redistribution of synaptic vesicles and their proteins in temperature-sensitive shibire(ts1) mutant Drosophila, Proc. Natl. Acad. Sci. USA 92 (1995) 5739–5743.
[10] B. Zhang, Y. Koh, R. Beckstead, V. Budnik, B. Ganetzky, H. Bellen, Synaptic vesicle size and number are regulated by a clathrin adaptor protein required for endocytosis, Neuron 21 (1998) 1465–1475.
[11] H. Zimmerman, V. Whittaker, Morphological and biochemical heterogeneity of cholinergic synaptic vesicles, Nature 267 (1977) 633–635.